The internal structure and dynamics of Jupiter unveiled by a high resolution magnetic field and secular variation model

S. Sharan[1], B. Langlais[1], H. Amit[1], E. Thébault[2], M. Pinceloup[1], and O. Verhoeven[1]

[1]Laboratoire de Planétologie et Géosciences, CNRS UMR 6112, Nantes Université, Université d'Angers, Le Mans Université, Nantes, France
[2]Laboratoire Magma et Volcans, Université Clermont Auvergne, UMR 6524, CNRS, IRD, OPGC, Clermont-Ferrand, France

Key Points:

- Magnetic field of Jupiter is modeled from Juno's first four years of observations
- A degree 13 magnetic field model and degree 8 secular variation model are derived
- The model indicates complex motions deep inside Jupiter

Corresponding author: Shivangi Sharan, `shivangi.sharan@univ-nantes.fr`

Corresponding author: Benoit Langlais, `benoit.langlais@univ-nantes.fr`

Abstract

Jupiter possesses the strongest magnetic field of all planets in the solar system. Modelling and interpreting this field gives essential information about the dynamo process acting at some depth inside Jupiter. Here we use the fluxgate magnetometer measurements acquired during the first four years of the Juno mission to derive an internal magnetic field and secular variation model using spherical harmonic functions. We compute an internal field model to degree 13, and a secular variation model to degree 8. The power spectrum of the field model is used to infer that the dynamo convective region has an upper boundary at 0.845±0.015 Jupiter radius, confirming that the transition layer plays a role in the field generation inside Jupiter. The secular variation timescales indicate that the dynamo is dominated by advective effects while the secular variation pattern suggests that the flow at the interior is complex and involves non-zonal features.

Plain Language Summary

The interior of Jupiter can be described broadly as a dense core surrounded by fluids, dominantly hydrogen and helium. The hydrogen rich metallic fluid generates the strongest planetary magnetic field in the Solar System. Modelling and interpreting this field gives essential information about the dynamo process inside Jupiter. We use the Juno mission data throughout four years to derive an internal magnetic field and secular variation (SV) model using spherical harmonic functions. We take the fluxgate magnetometer measurements acquired during the first 28 orbits to compute a magnetic field model to degree 13, and model its temporal variation to degree 8. The power spectrum of the magnetic field model is used to investigate the radius of the dynamo region. Using the non-zonal and quadrupole family spectra, we infer that the convective region has an upper boundary at 0.845±0.015 Jupiter radius. The slope of the SV timescales indicates that the dynamo is dominated by advective effects. The SV displays a maximum near the equator with a bi-polar structure in agreement with zonal drift of the Great Blue Spot. However, numerous small scale SV structures suggest that the flow at the interior is complex involving both zonal and non-zonal features.

1 Introduction

The interior of the giant planets of our Solar System can be described in simple terms as consisting of a core of unknown composition surrounded by fluid envelopes (Guillot, 2005). For Jupiter, the core could be small and dense, but also large and dilute (Wahl et al., 2017). The overlying envelopes consist of an inner layer of metallic hydrogen and an outer one of molecular hydrogen. Recent experimental results describe a transition H-He demixing layer, suggesting Helium rain between depths 0.68 and 0.84 R_J (Jupiter's equatorial radius, 1 R_J = 71,492 km) (Brygoo et al., 2021). The high temperature and pressure inside the planet renders it electrically conducting. Convection in the electrically conductive metallic hydrogen generates the strong Jovian magnetic field (Jones, 2011, 2014). In contrast to rocky bodies, Jupiter does not have an abrupt change between its metallic hydrogen (magnetic source) and molecular hydrogen (source free) regions. The change is expected to be gradual. The electrical conductivity profile of the different hydrogen layers at different depths from an ab-initio simulation (French et al., 2012) does not indicate a clear value of the dynamo region radius. Previous attempts to constrain this radius using the magnetic energy spectrum place it somewhere between 0.80 and 0.90 R_J (Langlais et al., 2014; Tsang & Jones, 2020; Connerney et al., 2022).

Jupiter's magnetic field has been measured by various flybys and orbiting satellites. The observations made by the flybys of Pioneer 10 and 11, Voyager 1 and 2 (during the seventies) and the Ulysses probe (early nineties) gave some initial information about the planet (Smith et al., 1974; Ness et al., 1979; Balogh et al., 1992). The first orbiting satellite, Galileo, was launched in 1989. It provided measurements from Jupiter and its moons from 1995 to 2003. Although these magnetic observations are spread over long periods of time, there have been only a few attempts to constrain or estimate the temporal variation of the field (Connerney et al., 1982; Yu et al., 2010; Ridley & Holme, 2016). Out of these studies, only Ridley and Holme (2016) co-estimated the secular variation (SV) with the main field (MF) using magnetic field measurements made between 1973 and 2003. However, due to the inhomogeneous temporal and geographical data distribution, most of the selected observations were from the Galileo mission at low latitudes. Ridley and Holme (2016) computed two models, one with only MF time averaged Gauss coefficients and one with time dependent MF and SV coefficients. The latter model was considered better because of its lower residuals and greater smoothness. Nevertheless, they considered their SV model to be reliable only up to degree 2.

None of these spacecrafts provided data near the poles. This was overcome by the recent Juno measurements. Juno space probe was launched on August 5th, 2011 and entered Jupiter's orbit in July 2016. Its magnetic measurements have already been used to propose new models of the Jovian field. Connerney et al. (2018) provided a spherical harmonic (SH) internal field model up to degree 10 using the initial 9 orbits. This initial model was improved by Connerney et al. (2022) who calculated a model up to degree 30 for internal and degree 1 for external, using the first 33 orbits. They state that the Gauss coefficients are well resolved until degree 13 though useful information can be retained until degree 18 for some coefficients. Jupiter's internal field is characterized by a very high magnitude, showing both dipole and non-dipole parts. The non-dipole field is dominantly observed in the northern hemisphere. Field change over a 45-year time span was observed and zonal drift was invoked to explain the temporal change of an intense magnetic flux patch near the equator (Moore et al., 2018, 2019). An updated external field magnetodisk model for Juno is also available (Connerney et al., 2020). None of the existing models based on Juno data attempt to model the current global temporal variation of the field.

In this study, we take advantage of the high quality Juno measurements to derive a high-resolution SH model of the Jovian field, simultaneously describing its MF and SV up to SH degrees 13 and 8 respectively. Section 2 details the data and the selection criteria we use for this study. Section 3 describes the method used to derive the models and their spectra. In Section 4 we analyze the model and discuss our results. We first determine the dynamo radius assuming white spectrum of specific parts of the field. We also calculate the SV correlation times of the Jovian field. We finally downward continue the field into Jupiter's interior and infer kinematic properties. We conclude in Section 5.

2 Data

Juno has a near polar, highly elliptical orbit with apojove exceeding over 100 Jupiter radii. The prime mission lasted five years and provided data for 33 orbits with one complete orbit taking about 53 days. The space probe was initially planned to undergo a reduction maneuver for achieving 14-day science orbits but Juno entered safe mode for its second orbit, thereby remaining in its initial 53-day capture orbit for the entire mission. The spacecraft aims to obtain a global coverage of the planet. For the first eight orbits, the shift between successive orbits was 45 degrees in longitude. The subsequent shifts reduce the longitudinal spacing by half to obtain data from the gaps left previously.

Juno uses two fluxgate magnetometers, located on one of the three solar arrays to measure the vector magnetic field. Magnetic field measurements acquired by Juno are available under two versions. The version 1 data provides measurements across the entire orbit, whereas the version 2 data gives only near planet measurements from the orbit, denoted as perijove hereafter. Both version 1 and 2 data are provided in three Cartesian coordinate systems - planetocentric, sun-state and payload. Since planetocentric system is body-fixed, it is the most appropriate to study the internal field. We use the version 2 one-second data in planetocentric coordinates from the first 28 perijoves (data available for only 27 perijoves, excluding the second one). As discussed later, adding more orbits leads to an increase in polar gaps that degrades the model. Perijove 19 was also dismissed because spurious oscillations were later observed.

The periapsis reaches altitude as low as 2500 km, or radius 1.03 Rj, and precesses about 1° in latitude northward, starting from the equator, after each orbit. In order to minimize external field contributions, we choose measurements near the planet's surface, i.e., all vector data below an arbitrarily chosen altitude of 300,000 km (or radius ∼5.2 R_J). The vector data range from August 2016 to July 2020 giving 628,828 data locations, that are plotted in Supporting Figure S1. Minimum measured field intensity is of the order of 3000 nT at maximum altitude, well above the 25 nT resolution of the magnetometer experiment, while the maximum intensity reaches above 10^6 nT.

3 Methodology

The magnetic field in a source free location can be expressed as the gradient of a scalar potential V that satisfies the Laplace equation:

$$\nabla^2 V = 0 \tag{1}$$

The potential for internal and external sources can be written as an expansion of SH functions:

$$\begin{aligned} V(r,\theta,\phi,t) &= a\sum_{n=1}^{n_{max}}\sum_{m=0}^{n}\left\{\left(\frac{a}{r}\right)^{n+1}\big(g_n^m(t)\cos m\phi + h_n^m(t)\sin m\phi\big)P_n^m\big(\cos\theta\big)\right\} \\ &\quad + a\sum_{n=1}^{n_{max}}\sum_{m=0}^{n}\left\{\left(\frac{r}{a}\right)^{n}\big(q_n^m(t)\cos m\phi + s_n^m(t)\sin m\phi\big)P_n^m\big(\cos\theta\big)\right\} \end{aligned} \tag{2}$$

where (r,θ,ϕ,t) are the planetocentric spherical coordinates (radius, co-latitude and longitude) and time, respectively. a is the reference radius equal to Jupiter's equatorial radius (71,492 km). $g_n^m(t)$ and $h_n^m(t)$ are the time-dependent internal field Gauss coefficients of degree n and order m while $q_n^m(t)$ and $s_n^m(t)$ are the external field coefficients. P_n^m are the Schmidt quasi-normalised associated Legendre functions.

The choice of data near the surface allows to minimise the external field contribution and restrict its description up to degree 2. To calculate the SH coefficients, we apply a standard least-square inversion approach to the data that aims to minimise the differences between the measurements and the predictions by the model. We use constant weights, set to the magnetometer resolution of 25 nT. The temporal variation of the internal field is calculated using B-splines of order 2. B-splines are piecewise polynomials that calculate derivatives using augmented knots, which are the pieces that are produced in the polynomial. We define two boundary knots using the time interval of our data and augment the knot sequence using the mean. Details of the method and tests applied on the dataset are provided in the Supporting Information.

The Lowes-Mauersberger spectrum represents the magnetic field power spectrum per SH degree (Mauersberger, 1956; Lowes, 2007). For a given time, and at a given radius r, it can be defined as

$$\mathcal{R}_n = (n+1)\left(\frac{a}{r}\right)^{(2n+4)}\sum_{m=0}^{n}[(g_n^m)^2 + (h_n^m)^2] \tag{3}$$

at SH degree n. Similarly, for the SV, it can be defined as

$$\mathcal{S}_n = (n+1)\left(\frac{a}{r}\right)^{(2n+4)} \sum_{m=0}^{n} [(\dot{g}_n^m)^2 + (\dot{h}_n^m)^2] \tag{4}$$

where $\dot{g}_n^m$ and $\dot{h}_n^m$ are the Gauss coefficients of the SV.

The main field and its spectrum $\mathcal{R}_n$ can be upward or downward continued, provided there are no magnetic field sources present in between. This property has been used to derive estimates of the radius of the dynamo region, or of the liquid core in the case of the Earth. This is also known as the white noise hypothesis: immediately outside the dynamo region, the part of the magnetic spectrum associated with the dynamo becomes flat, and the depth to the dynamo can thus be grossly estimated (Lowes, 1974). However some terms (n=1 and n=2) have to be removed or ignored in order for this approximation to match the radius of the Earth's core (Cain et al., 1989; Voorhies, 2004). Langlais et al. (2014) found that certain parts of the spectrum $\mathcal{R}_n$, the non-zonal and quadrupole family, are independent of n at some radius r (see Supporting Information for details). On Earth, these more rigorous approaches return the value of the core or dynamo radius with a combined relative error lower than 0.3%. In the following, we refer to this radius as $\mathbf{R}_{sf}$. It can be interpreted as the radius of the top of the source region, or the bottom of the source free region.

Finally, the correlation times as a function of degree n can be defined, combining the quantities $\mathcal{R}_n$ and $\mathcal{S}_n$. The correlation times, also referred to as the SV timescales, give a measure of how long it takes for the field of a particular degree to get reorganized, or become uncorrelated to its former state at that degree (Hulot & Le Mouël, 1994; Christensen & Tilgner, 2004; Amit et al., 2018). It is expressed as

$$\tau_n = \sqrt{\frac{\mathcal{R}_n}{\mathcal{S}_n}} \tag{5}$$

4 Results and Discussion

We calculate the main field model up to degree 20 and the SV to degree 8. The external field is estimated up to degree 2. The power spectrum of the main field at Jupiter's surface decreases up to $n = 13$ (Figure 1a). We notice an increase from $n = 13$ to 16 possibly due to data distribution and aliasing as suggested by our synthetic analyzes (see Supporting Information). With increasing orbits, the satellite goes lower in altitude near the north pole while increasing the size of a gap at similar latitude over the south pole area. This results in high degree, low order terms not being well resolved (i.e., zonal and near zonal terms). This effect can be seen in the south polar cap. Hence, we truncate our field model at $n_{max} = 13$ while retaining $n_{max} = 8$ for the SV model. The unweighted misfits, given by the root mean square of the residuals for the different components for our model and a model calculated without SV are given in Supporting Table S1. They indicate that the model with SV is superior since the misfit for the field intensity decreases by 2.6%. The Supporting Figure S2 shows the misfits for our model, a model calculated without SV and the model by Connerney et al. (2022). All values and figures presented are calculated at the central epoch of the data (August 2018).

4.1 Inferences on the internal structure

Using the power spectrum, we calculate $\mathbf{R}_{sf}$ for varying n_{max}. The radius notably remains stable until $n_{max} = 13$ while it starts to increase from $n_{max} = 14$ (see Supporting Information). This confirms our maximal reliable degree choice for the main field model. We use the mean of the radius values obtained from the non-zonal ($m \neq 0$) and quadrupole family (n+m even) terms up to degree 13 as defined by Langlais et al. (2014).

The value from the non-zonal field is 0.851 R_J and that from the quadrupole family is 0.839 R_J, which together give a mean of 0.845 R_J with a standard deviation of 0.015 R_J. Previous results give similar values. Connerney et al. (2018) estimate the dynamo radius 'near 0.85 R_J' while Connerney et al. (2022) estimate it to 0.81 R_J. Tsang and Jones (2020) estimate it between 0.82 and 0.87 R_J using a numerical model. However, all these studies use the white noise hypothesis as discussed above, which ignores the $n = 1$ and even $n = 2$ terms. Our result $\mathbf{R}_{sf} = 0.845\ R_J$ is more accurate and offers more robust constraints on the interior and dynamics of Jupiter.

For a dynamo to exist in a planet, two main criteria are required: an electrically-conducting fluid and an energy source, which is often convection within a spherical shell in rotation. For Jupiter, the metallic hydrogen is the fluid, and its convective motion drives the dynamo. Convection can also take place in the source free region, without contributing to the dynamo. Wicht and Gastine (2020), through numerical simulations, suggested the possibility of two distinct dynamo regions inside Jupiter. The primary region would be at depth, and is responsible for the dipole dominated field geometry. The secondary one would be shallower, and operates where the equatorial jets encounter conductive material in the transition layer. However, surface jets motion decays rapidly with depth and are unlikely to extend at depths larger than about 3,000-3,500 km or ∼0.95 R_J (Kaspi et al., 2018; Guillot et al., 2018). Christensen et al. (2020) suggested that a stratified layer, close to the surface, could quench the jets at depth and play a role in the secondary dynamo. Our study points towards a source free region extending deeper, with a radius placed at 0.845 R_J. This radius could correspond to the upper limit of the dynamo region. We note that it also matches well the radius of the transition layer in between the metallic and molecular hydrogen (Brygoo et al., 2021), rendering this layer part of the dynamo region (Figure 2). Our results do not provide constraints on the bottom radius of the dynamo and do not indicate a shallower secondary dynamo (Gastine & Wicht, 2021) above 0.845 R_J.

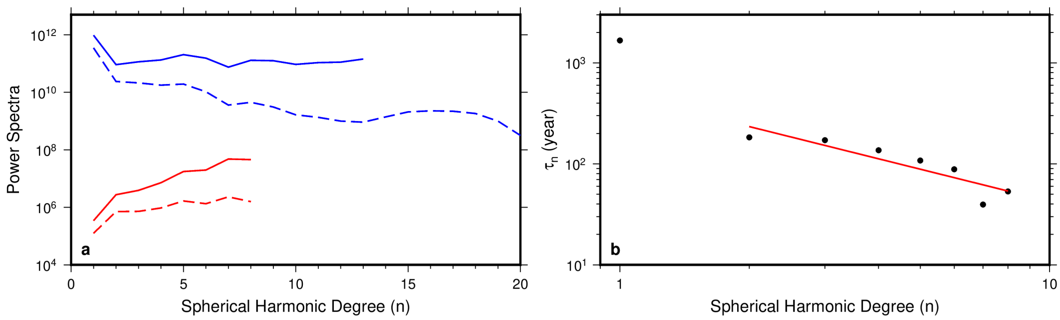

Figure 1. (**a**) The power spectra of the main field (shown in blue, units - nT^2) and secular variation (shown in red, units - $(nT/year)^2$) of the model at the surface (dashed line) and at $\mathbf{R}_{sf}$ (solid line). The main field terms for $n > 13$ are not downward continued to $\mathbf{R}_{sf}$. (**b**) The secular variation timescales of the model. The red line in (**b**) is the linear best fit to the non-dipole part.

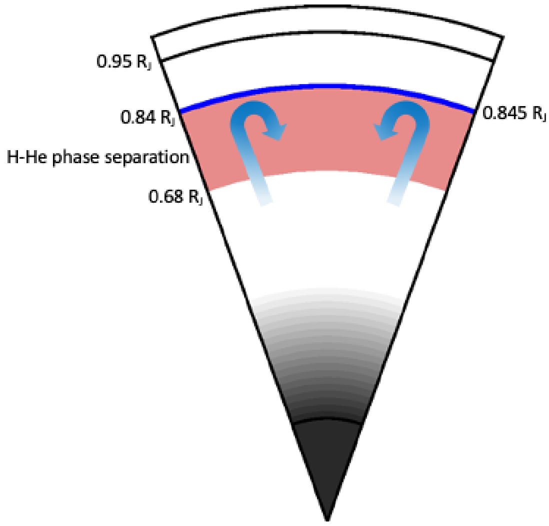

Figure 2. Schematic view of the interior of Jupiter. The blue line depicts our result $\mathbf{R}_{sf}$. The grey area depicts the core (0.2 R_J) and the possible dilute core region (Wicht & Gastine, 2020; Wahl et al., 2017). The red area depicts the H-He phase separated layer (Brygoo et al., 2021). The 0.95 R_J depicts the depth where the jets decay down to the minimum (Kaspi et al., 2018). The arrows represent possible convection area with unknown origin depth.

4.2 SV Timescales

The SV timescales are shown in Figure 1b. For the Earth, the correlation time for the dipole is around 1000 years and the lowest value at $\sim n_{max} = 13$ is of the order of 10 years. Field models and numerical dynamo simulations indicate that the non-dipole SV timescales are inversely proportional to the SH degree (e.g., Lhuillier et al., 2011; Bouligand et al., 2016). For Jupiter, the correlation time for the dipole (τ_1) is 1667 years while the lowest value we obtain is 40 years for degree 7. We observe similar inverse proportionality for the Jovian SV timescales. The best fit slope for $n = 2 - 8$ is -1.06 with a standard deviation of 0.23. According to the scaling theory of the magnetic induction equation, a slope of -1 corresponds to advective SV, whereas -2 indicates diffusive SV (Christensen et al., 2012; Holme & Olsen, 2006). A -2 slope for our model is well outside 2 standard deviations and can be excluded. Therefore, our best fit value -1.06$\pm$0.23 suggests that the field change is dominated by advective effects, as is the case for Earth (Lhuillier et al., 2011; Christensen et al., 2012).

In addition, the overall similarity between the non-dipole SV timescales of Jupiter and Earth suggests a similar magnetic Reynolds number (Christensen & Tilgner, 2004), i.e. $Rm_J \sim 1000$. In contrast, Wicht et al. (2019) concluded that diffusive effects might govern the dynamo in the transition layer. Though their transition region starts above $\mathbf{R}_{sf}$, the SV timescales we compute are independent of the radius, hence challenging the importance of diffusion. It thus remains an open question as to what phenomenon drives the observed SV of Jupiter.

4.3 Implications to Jupiter's dynamo

Using the four morphological criteria defined in Christensen et al. (2010) for Earth-like dynamo models at the CMB, we compare our results with the geodynamo. For comparison purposes, we set $n_{max} = 8$ to calculate the different criteria, i.e. smaller than that shown in Figure 3(a-f). The relative axial dipole power for our model is 0.99 at $\mathbf{R}_{sf}$ while the standard value for Earth is 1.4, though the present-day value is about 1. This indicates that Jupiter's dynamo is either less dipolar or comparable to Earth's (Figures 3a and 3b). The equatorial anti-symmetry for Earth is 1.0, whereas our model provides a value of 0.54. A random equipartitioned non-dipole field ratio would give an equatorial anti-symmetry of 0.83 (Christensen et al., 2010). Thus, Jupiter's non-dipole field is more symmetric with respect to the equator than Earth's (Figures 3c and 3d). The zonal to non-zonal ratio for a random equipartitioned field is 0.10 (Christensen et al., 2010). For Earth, the value is 0.15, while for our model the value is 0.19, which indicates a stronger zonal contribution (Figures 3e and 3f). Lastly, the flux concentration for a purely dipole field is 0.8 and that for the geomagnetic field is 1.50 (Christensen et al., 2010). The flux concentration is considered low when flux exits one hemisphere and enters through the other uniformly. Conversely, it is large when it exits from a concentrated spot and enters the rest of the sphere uniformly. The concentration value for our model is 4.0. This very large value reflects the dominance of the large intense flux patch in the northern hemisphere.

Figure 4 shows the radial magnetic field and SV maps calculated using the model at Jupiter's surface and at $\mathbf{R}_{sf}$. The large positive radial field patch in the northern hemisphere and the intense negative patch near the equator (the Great Blue Spot) become more concentrated with depth. SV is of the order of 10^4 nT/year at the surface. This corresponds to a 2.4% change over the course of four years of the dataset used, compared to the 1.4% change over a similar duration for the Earth's magnetic field. As for the Earth's, it should not be ignored when modelling the magnetic field over periods exceeding a few years.

The spatial pattern of temporal variation of the field brings further dynamical constraints. The power spectrum of the SV calculated at $\mathbf{R}_{sf}$ increases with degree (Figure 1a). Indeed, the SV reveals intense small scale structures (Figure 4). The strong negative radial field patch immediately south of the equator (Figure 4b) coincides with a pair of SV structures (Figure 4d), suggesting eastward drift (Amit, 2014; Livermore et al., 2017). This is opposite to the westward drifting low- and mid-latitude patches observed with Earth's SV (Bullard et al., 1950; Finlay & Jackson, 2003; Aubert et al., 2013). This eastward drift could relate to the zonal winds observed at the surface or until 0.95 R_J (Moore et al., 2019). However, our model presents also other prominent SV structures which cannot be explained by zonal winds. There is some suggestion for a weak eastward drift near 45°N latitude, which is the centre of the large positive radial field patch (Figure 4b). But, it is not associated with particularly strong SV for most of its structure, possibly indicating a region with dominantly field-aligned flow (Finlay & Amit, 2011). Livermore et al. (2017) gave similar explanation for the absence of strong SV at southern high latitudes of Earth. Bearing in mind that the model is less constrained at the south pole, the opposite signs of B_r and $\dot{B}_r$ (Supporting Figure S3) suggest local fluid upwelling (Amit, 2014), similar to the field and SV below Earth's poles and in agreement with a classic meridional circulation inside the tangent cylinder (Olson & Aurnou, 1999; Cao et al., 2018). In addition, the southern hemisphere has many alternating sign SV patches (Figure 4d) which are not correlated with particularly strong field structures (Figure 4b). We note that the radial field and its SV from $\mathbf{R}_{sf}$ to the surface are weakly sensitive to depth (Figure 4), making these kinematic interpretations robust.

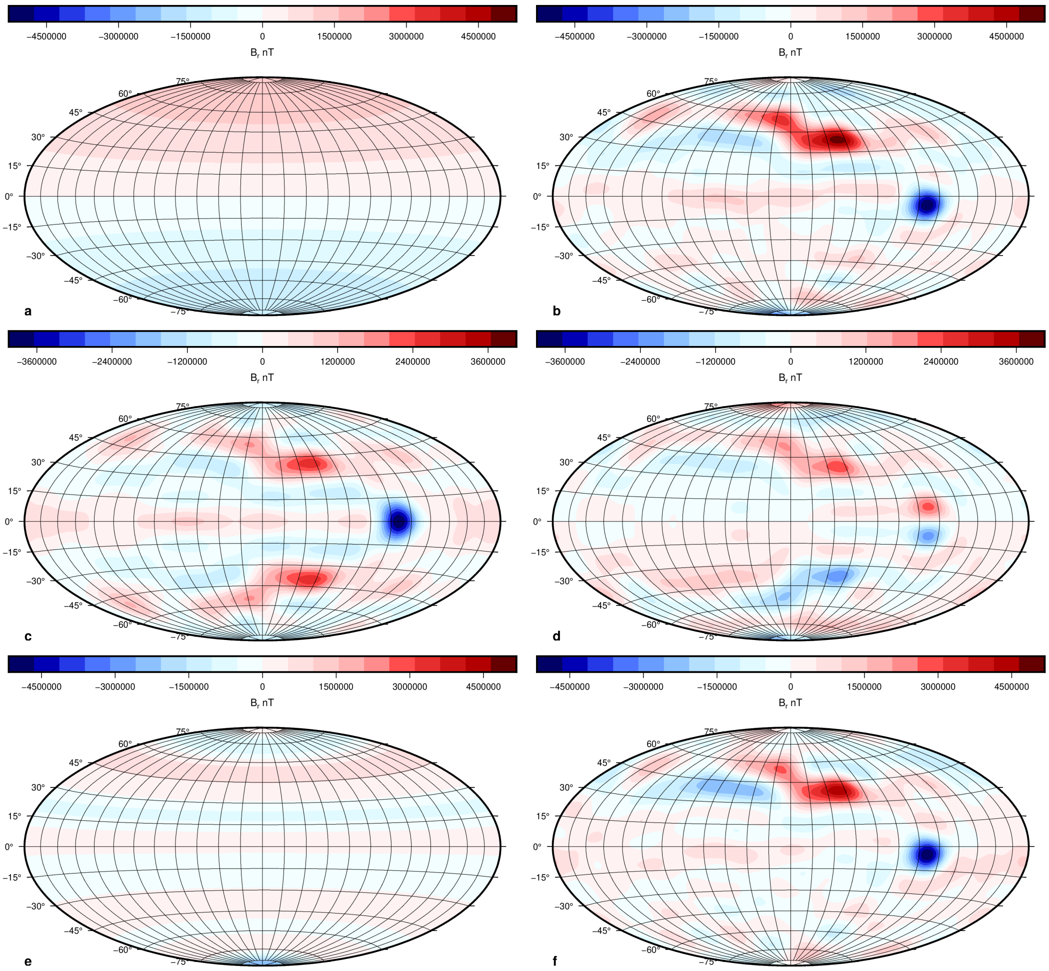

Figure 3. The radial field at $\mathbf{R}_{sf}$. (**a**) Axial dipole field. (**b**) Non axial dipole field. (**c**) Non-dipole symmetric field. (**d**) Non-dipole anti-symmetric field. (**e**) Non-dipole zonal field. (**f**) Non-dipole non-zonal field.

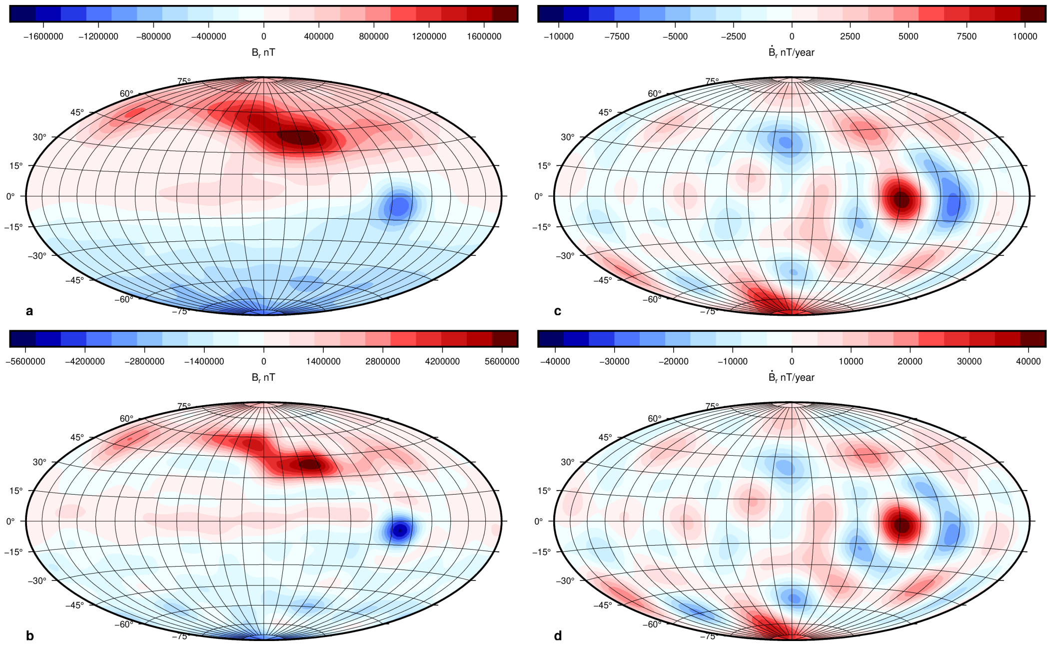

Figure 4. The (**a, b**) radial field and (**c, d**) its secular variation at (top) Jupiter's surface and (bottom) $\mathbf{R}_{sf}$.

5 Concluding remarks

We present a magnetic field model robust up to degree 13 and secular variation up to degree 8. The dynamo radius of 0.845 R_J is more precise considering the method used and indicates that the transition region is part of the dynamo generation. The dominance of advective SV and the relative level of axial dipolarity of Jupiter exhibit similarity with the geodynamo. We find that the global secular variation is not weak enough to be neglected and the flow deep inside Jupiter involves zonal as well as complex non-zonal structures.

More insights into the dynamo regime could be gleaned by inferring the flow at Jupiter's deep interior. Our field and SV model can be inverted for the flow at $\mathbf{R}_{sf}$. Such an inversion, which is commonly performed for the flow at the top of Earth's core (Holme, 2015), was performed for Jupiter by Ridley and Holme (2016), but using a very low resolution SV model. More data are also needed to increase the resolution of the field model and to confirm the temporal variation observed during the last four years. This will come from Juno during the upcoming extended mission, but also when the ESA's JUICE mission enters Jupiter's orbit at the end of this decade.

Open Research

All Juno magnetometer data used here are publicly available on NASA's Planetary Data System (PDS) at Planetary Plasma Interactions (PPI) node at

`https://pds-ppi.igpp.ucla.edu/search/?sc=Juno&t=Jupiter&i=FGM`.

`https://pds-ppi.igpp.ucla.edu/search/view/?f=yes&id=pds://PPI/JNO-J-3-FGM-CAL-V1.0/DATA/JUPITER/PC`.

References

Alken, P., Thébault, E., Beggan, C. D., Aubert, J., Baerenzung, J., Brown, W. J., ... Wardinski, I. (2021). Evaluation of candidate models for the 13th generation international geomagnetic reference field. *Earth, Planets and Space*, *73*(1), 48. Retrieved from https://doi.org/10.1186/s40623-020-01281-4 doi: 10.1186/s40623-020-01281-4

Amit, H. (2014). Can downwelling at the top of the earth's core be detected in the geomagnetic secular variation? *Physics of the Earth and Planetary Interiors*, *229*, 110-121. Retrieved from https://www.sciencedirect.com/science/article/pii/S0031920114000132 doi: https://doi.org/10.1016/j.pepi.2014.01.012

Amit, H., Coutelier, M., & Christensen, U. R. (2018). On equatorially symmetric and antisymmetric geomagnetic secular variation timescales. *Physics of the Earth and Planetary Interiors*, *276*, 190-201. Retrieved from https://www.sciencedirect.com/science/article/pii/S0031920116302898 (Special Issue:15th SEDI conference) doi: https://doi.org/10.1016/j.pepi.2017.04.009

Aubert, J., & Finlay, C. C. (2019). Geomagnetic jerks and rapid hydromagnetic waves focusing at earth's core surface. *Nature Geoscience*, *12*(5), 393–398. Retrieved from https://doi.org/10.1038/s41561-019-0355-1 doi: 10.1038/s41561-019-0355-1

Aubert, J., Finlay, C. C., & Fournier, A. (2013). Bottom-up control of geomagnetic secular variation by the earth's inner core. *Nature*, *502*(7470), 219–223. Retrieved from https://doi.org/10.1038/nature12574 doi: 10.1038/nature12574

Balogh, A., Dougherty, M. K., Forsyth, R. J., Southwood, D. J., Smith, E. J., Tsurutani, B. T., ... Burton, M. E. (1992). Magnetic field observations during the ulysses flyby of jupiter. *Science*, *257*(5076), 1515-1518. Retrieved from https://www.science.org/doi/abs/10.1126/science.257.5076.1515 doi: 10.1126/science.257.5076.1515

Bouligand, C., Gillet, N., Jault, D., Schaeffer, N., Fournier, A., & Aubert, J. (2016, 09). Frequency spectrum of the geomagnetic field harmonic coefficients from dynamo simulations. *Geophysical Journal International*, *207*(2), 1142-1157. Retrieved from https://doi.org/10.1093/gji/ggw326 doi: 10.1093/gji/ggw326

Brygoo, S., Loubeyre, P., Millot, M., Rygg, J. R., Celliers, P. M., Eggert, J. H., ... Collins, G. W. (2021). Evidence of hydrogen-helium immiscibility at jupiter-interior conditions. *Nature*, *593*(7860), 517–521. Retrieved from https://doi.org/10.1038/s41586-021-03516-0 doi: 10.1038/s41586-021-03516-0

Bullard, E. C., Freedman, C., Gellman, H., & Nixon, J. (1950). The westward drift of the earth's magnetic field. *Philosophical Transactions of the Royal Society of London. Series A, Mathematical and Physical Sciences*, *243*(859), 67-92. Retrieved from https://royalsocietypublishing.org/doi/abs/10.1098/rsta.1950.0014 doi: 10.1098/rsta.1950.0014

Cain, J. C., Wang, Z., Schmitz, D. R., & Meyer, J. (1989, 06). The geomagnetic spectrum for 1980 and core-crustal separation. *Geophysical Journal International*, *97*(3), 443-447. Retrieved from https://doi.org/10.1111/j.1365-246X.1989.tb00514.x doi: 10.1111/j.1365-246X.1989.tb00514.x

Cao, H., Yadav, R. K., & Aurnou, J. M. (2018). Geomagnetic polar minima do not arise from steady meridional circulation. *Proceedings of the National Academy of Sciences*, *115*(44), 11186–11191. Retrieved from https://www.pnas.org/content/115/44/11186 doi: 10.1073/pnas.1717454115

Christensen, U. R., Aubert, J., & Hulot, G. (2010). Conditions for earth-like geodynamo models. *Earth and Planetary Science Letters*, *296*(3), 487-496. Retrieved from https://www.sciencedirect.com/science/article/pii/S0012821X10003833 doi: https://doi.org/10.1016/j.epsl.2010.06.009

Christensen, U. R., & Tilgner, A. (2004). Power requirement of the geodynamo from ohmic losses in numerical and laboratory dynamos. *Nature*, *429*(6988), 169–171. Retrieved from https://doi.org/10.1038/nature02508 doi: 10.1038/nature02508

Christensen, U. R., Wardinski, I., & Lesur, V. (2012, 07). Timescales of geomagnetic secular acceleration in satellite field models and geodynamo models. *Geophysical Journal International*, *190*(1), 243-254. Retrieved from https://doi.org/10.1111/j.1365-246X.2012.05508.x doi: 10.1111/j.1365-246X.2012.05508.x

Christensen, U. R., Wicht, J., & Dietrich, W. (2020, feb). Mechanisms for limiting the depth of zonal winds in the gas giant planets. *The Astrophysical Journal*, *890*(1), 61. Retrieved from https://doi.org/10.3847/1538-4357/ab698c doi: 10.3847/1538-4357/ab698c

Connerney, J. E. P., Acuña, M. H., & Ness, N. F. (1982). Voyager 1 assessment of jupiter's planetary magnetic field. *Journal of Geophysical Research: Space Physics*, *87*(A5), 3623-3627. Retrieved from https://agupubs.onlinelibrary.wiley.com/doi/abs/10.1029/JA087iA05p03623 doi: https://doi.org/10.1029/JA087iA05p03623

Connerney, J. E. P., Kotsiaros, S., Oliversen, R. J., Espley, J. R., Joergensen, J. L., Joergensen, P. S., ... Levin, S. M. (2018). A new model of jupiter's magnetic field from juno's first nine orbits. *Geophysical Research Letters*, *45*(6), 2590-2596. Retrieved from https://agupubs.onlinelibrary.wiley.com/doi/abs/10.1002/2018GL077312 doi: https://doi.org/10.1002/2018GL077312

Connerney, J. E. P., Timmins, S., Herceg, M., & Joergensen, J. L. (2020). A jovian magnetodisc model for the juno era. *Journal of Geophysical Research: Space Physics*, *125*(10), e2020JA028138. Retrieved from https://agupubs.onlinelibrary.wiley.com/doi/abs/10.1029/2020JA028138 (e2020JA028138 2020JA028138) doi: https://doi.org/10.1029/2020JA028138

Connerney, J. E. P., Timmins, S., Oliversen, R. J., Espley, J. R., Joergensen, J. L., Kotsiaros, S., ... Levin, S. M. (2022). A new model of jupiter's magnetic field at the completion of juno's prime mission. *Journal of Geophysical Research: Planets*, *127*(2), e2021JE007055. Retrieved from https://agupubs.onlinelibrary.wiley.com/doi/abs/10.1029/2021JE007055 (e2021JE007055 2021JE007055) doi: https://doi.org/10.1029/2021JE007055

de Boor, C. (2001). Calculation of the smoothing spline with weighted roughness measure. *Mathematical Models and Methods in Applied Sciences*, *11*(01), 33-41. Retrieved from https://doi.org/10.1142/S0218202501000726 doi: 10.1142/S0218202501000726

Finlay, C. C., & Amit, H. (2011, 07). On flow magnitude and field-flow alignment at Earth's core surface. *Geophysical Journal International*, *186*(1), 175-192. Retrieved from https://doi.org/10.1111/j.1365-246X.2011.05032.x doi: 10.1111/j.1365-246X.2011.05032.x

Finlay, C. C., & Jackson, A. (2003). Equatorially dominated magnetic field change at the surface of earth's core. *Science*, *300*(5628), 2084–2086. Retrieved from https://science.sciencemag.org/content/300/5628/2084 doi: 10.1126/science.1083324

Finlay, C. C., Kloss, C., Olsen, N., Hammer, M. D., Tøffner-Clausen, L., Grayver, A., & Kuvshinov, A. (2020). The chaos-7 geomagnetic field model and observed changes in the south atlantic anomaly. *Earth, Planets and Space*, *72*(1), 156. Retrieved from https://doi.org/10.1186/s40623-020-01252-9 doi: 10.1186/s40623-020-01252-9

French, M., Becker, A., Lorenzen, W., Nettelmann, N., Bethkenhagen, M., Wicht, J., & Redmer, R. (2012, aug). Ab initio simulations for material properties along the jupiter adiabat. *The Astrophysical Journal Supplement Series*, *202*(1), 5. Retrieved from https://doi.org/10.1088/0067-0049/202/1/5 doi:

10.1088/0067-0049/202/1/5

Gastine, T., & Wicht, J. (2021). Stable stratification promotes multiple zonal jets in a turbulent jovian dynamo model. *Icarus*, *368*, 114514. Retrieved from https://www.sciencedirect.com/science/article/pii/S0019103521001895 doi: https://doi.org/10.1016/j.icarus.2021.114514

Guillot, T. (2005). The interiors of giant planets: Models and outstanding questions. *Annual Review of Earth and Planetary Sciences*, *33*(1), 493-530. Retrieved from https://doi.org/10.1146/annurev.earth.32.101802.120325 doi: 10.1146/annurev.earth.32.101802.120325

Guillot, T., Miguel, Y., Militzer, B., Hubbard, W. B., Kaspi, Y., Galanti, E., ... Bolton, S. J. (2018). A suppression of differential rotation in jupiter's deep interior. *Nature*, *555*(7695), 227–230. Retrieved from https://doi.org/10.1038/nature25775 doi: 10.1038/nature25775

Holme, R. (2015, 01). Large-scale flow in the core. In (p. 91-113). doi: 10.1016/B978-0-444-53802-4.00138-X

Holme, R., & Olsen, N. (2006, 08). Core surface flow modelling from high-resolution secular variation. *Geophysical Journal International*, *166*(2), 518-528. Retrieved from https://doi.org/10.1111/j.1365-246X.2006.03033.x doi: 10.1111/j.1365-246X.2006.03033.x

Hulot, G., & Le Mouël, J. (1994). A statistical approach to the earth's main magnetic field. *Physics of the Earth and Planetary Interiors*, *82*(3), 167-183. Retrieved from https://www.sciencedirect.com/science/article/pii/0031920194900701 doi: https://doi.org/10.1016/0031-9201(94)90070-1

Jones, C. A. (2011). Planetary magnetic fields and fluid dynamos. *Annual Review of Fluid Mechanics*, *43*(1), 583-614. Retrieved from https://doi.org/10.1146/annurev-fluid-122109-160727 doi: 10.1146/annurev-fluid-122109-160727

Jones, C. A. (2014). A dynamo model of jupiter's magnetic field. *Icarus*, *241*, 148-159. Retrieved from https://www.sciencedirect.com/science/article/pii/S0019103514003315 doi: https://doi.org/10.1016/j.icarus.2014.06.020

Kaspi, Y., Galanti, E., Hubbard, W. B., Stevenson, D. J., Bolton, S. J., Iess, L., ... Wahl, S. M. (2018). Jupiter's atmospheric jet streams extend thousands of kilometres deep. *Nature*, *555*(7695), 223–226. Retrieved from https://doi.org/10.1038/nature25793 doi: 10.1038/nature25793

Langlais, B., Amit, H., Larnier, H., Thébault, E., & Mocquet, A. (2014). A new model for the (geo)magnetic power spectrum, with application to planetary dynamo radii. *Earth and Planetary Science Letters*, *401*, 347-358. Retrieved from https://www.sciencedirect.com/science/article/pii/S0012821X14003070 doi: https://doi.org/10.1016/j.epsl.2014.05.013

Lhuillier, F., Fournier, A., Hulot, G., & Aubert, J. (2011). The geomagnetic secular-variation timescale in observations and numerical dynamo models. *Geophysical Research Letters*, *38*(9). Retrieved from https://agupubs.onlinelibrary.wiley.com/doi/abs/10.1029/2011GL047356 doi: https://doi.org/10.1029/2011GL047356

Livermore, P. W., Hollerbach, R., & Finlay, C. C. (2017). An accelerating high-latitude jet in earth's core. *Nature Geoscience*, *10*(1), 62–68. Retrieved from https://doi.org/10.1038/ngeo2859 doi: 10.1038/ngeo2859

Lowes, F. J. (1966). Mean-square values on sphere of spherical harmonic vector fields. *Journal of Geophysical Research (1896-1977)*, *71*(8), 2179-2179. Retrieved from https://agupubs.onlinelibrary.wiley.com/doi/abs/10.1029/JZ071i008p02179 doi: https://doi.org/10.1029/JZ071i008p02179

Lowes, F. J. (1974, 03). Spatial power spectrum of the main geomagnetic field, and extrapolation to the core. *Geophysical Journal International*, *36*(3), 717-730. Retrieved from https://doi.org/10.1111/j.1365-246X.1974.tb00622.x doi: 10.1111/j.1365-246X.1974.tb00622.x

Lowes, F. J. (2007). Geomagnetic spectrum, spatial. In D. Gubbins & E. Herrero-

Bervera (Eds.), *Encyclopedia of geomagnetism and paleomagnetism* (pp. 350–353). Dordrecht: Springer Netherlands. Retrieved from https://doi.org/10.1007/978-1-4020-4423-6_126 doi: 10.1007/978-1-4020-4423-6_126

Mauersberger, P. (1956). Das mittel der energiedichte des geomagnetischen hauptfeldes an der erdoberflache und seine saulare anderung. *Gerlands Beitr. Geophys.*, *65*, 207-215. Retrieved from https://ci.nii.ac.jp/naid/10006217427/en/

McLeod, M. G. (1996). Spatial and temporal power spectra of the geomagnetic field. *Journal of Geophysical Research: Solid Earth*, *101*(B2), 2745-2763. Retrieved from https://agupubs.onlinelibrary.wiley.com/doi/abs/10.1029/95JB03042 doi: https://doi.org/10.1029/95JB03042

Moore, K. M., Cao, H., Bloxham, J., Stevenson, D. J., Connerney, J. E. P., & Bolton, S. J. (2019). Time variation of jupiter's internal magnetic field consistent with zonal wind advection. *Nature Astronomy*, *3*(8), 730–735. Retrieved from https://doi.org/10.1038/s41550-019-0772-5 doi: 10.1038/s41550-019-0772-5

Moore, K. M., Yadav, R. K., Kulowski, L., Cao, H., Bloxham, J., Connerney, J. E. P., ... Levin, S. M. (2018). A complex dynamo inferred from the hemispheric dichotomy of jupiter's magnetic field. *Nature*, *561*(7721), 76–78. Retrieved from https://doi.org/10.1038/s41586-018-0468-5 doi: 10.1038/s41586-018-0468-5

Ness, N. F., Acuna, M. H., Lepping, R. P., Burlaga, L. F., Behannon, K. W., & Neubauer, F. M. (1979, Jun). Magnetic field studies at jupiter by voyager 1: preliminary results. *Science*, *204*(4396), 982–987. doi: 10.1126/science.204.4396.982

Olson, P., & Aurnou, J. (1999). A polar vortex in the earth's core. *Nature*, *402*(6758), 170–173. Retrieved from https://doi.org/10.1038/46017 doi: 10.1038/46017

Ridley, V. A., & Holme, R. (2016). Modeling the jovian magnetic field and its secular variation using all available magnetic field observations. *Journal of Geophysical Research: Planets*, *121*(3), 309-337. Retrieved from https://agupubs.onlinelibrary.wiley.com/doi/abs/10.1002/2015JE004951 doi: https://doi.org/10.1002/2015JE004951

Smith, E. J., Davis Jr., L., Jones, D. E., Coleman Jr., P. J., Colburn, D. S., Dyal, P., ... Frandsen, A. M. A. (1974). The planetary magnetic field and magnetosphere of jupiter: Pioneer 10. *Journal of Geophysical Research (1896-1977)*, *79*(25), 3501-3513. Retrieved from https://agupubs.onlinelibrary.wiley.com/doi/abs/10.1029/JA079i025p03501 doi: https://doi.org/10.1029/JA079i025p03501

Tsang, Y.-K., & Jones, C. A. (2020). Characterising jupiter's dynamo radius using its magnetic energy spectrum. *Earth and Planetary Science Letters*, *530*, 115879. Retrieved from https://www.sciencedirect.com/science/article/pii/S0012821X19305710 doi: https://doi.org/10.1016/j.epsl.2019.115879

Voorhies, C. V. (2004). Narrow-scale flow and a weak field by the top of earth's core: Evidence from Ørsted, magsat, and secular variation. *Journal of Geophysical Research: Solid Earth*, *109*(B3). Retrieved from https://agupubs.onlinelibrary.wiley.com/doi/abs/10.1029/2003JB002833 doi: https://doi.org/10.1029/2003JB002833

Wahl, S. M., Hubbard, W. B., Militzer, B., Guillot, T., Miguel, Y., Movshovitz, N., ... others (2017). Comparing jupiter interior structure models to juno gravity measurements and the role of a dilute core. *Geophysical Research Letters*, *44*(10), 4649–4659.

Wicht, J., & Gastine, T. (2020). Numerical simulations help revealing the dynamics underneath the clouds of jupiter. *Nature Communications*, *11*(1), 2886. Retrieved from https://doi.org/10.1038/s41467-020-16680-0 doi: 10.1038/

s41467-020-16680-0
Wicht, J., Gastine, T., & Duarte, L. D. V. (2019). Dynamo action in the steeply decaying conductivity region of jupiter-like dynamo models. *Journal of Geophysical Research: Planets*, *124*(3), 837-863. Retrieved from https://agupubs.onlinelibrary.wiley.com/doi/abs/10.1029/2018JE005759 doi: https://doi.org/10.1029/2018JE005759
Yu, Z. J., Leinweber, H. K., & Russell, C. T. (2010, 2021/06/28). Galileo constraints on the secular variation of the jovian magnetic field. *Journal of Geophysical Research: Planets*, *115*(E3). Retrieved from https://doi.org/10.1029/2009JE003492 doi: https://doi.org/10.1029/2009JE003492

6 References for Supporting Information

(Finlay et al., 2020) (de Boor, 2001) (Aubert & Finlay, 2019) (Alken et al., 2021) (Lowes, 1966) (Lowes, 1974) (McLeod, 1996)